Chemistry and Physics of Lipids 160 (2009) 33–44

Contents lists available at ScienceDirect

Chemistry and Physics of Lipids

journal homepage: www.elsevier.com/locate/chemphyslip

Effects of ether vs. ester linkage on lipid bilayer structure and water permeability

S. Deren Guler[a], D. Dipon Ghosh[b], Jianjun Pan[a], John C. Mathai[c], Mark L. Zeidel[c], John F. Nagle[a,b], Stephanie Tristram-Nagle[a,*]

[a] Department of Physics, Carnegie Mellon University, Pittsburgh, PA 15213, USA
[b] Department of Biological Sciences, Carnegie Mellon University, Pittsburgh, PA 15213, USA
[c] Department of Medicine, Beth Israel Deaconess Medical Center and Harvard Medical School, Cambridge, MA 02139, USA

ARTICLE INFO

Article history:
Received 29 January 2009
Received in revised form 29 March 2009
Accepted 26 April 2009
Available online 3 May 2009

Keywords:
Ether lipid
X-ray
Structure
Water permeability
Lipid bilayers

ABSTRACT

The structure and water permeability of bilayers composed of the ether-linked lipid, dihexadecylphosphatidylcholine (DHPC), were studied and compared with the ester-linked lipid, dipalmitoylphosphatidylcholine (DPPC). Wide angle X-ray scattering on oriented bilayers in the fluid phase indicate that the area per lipid A is slightly larger for DHPC than for DPPC. Low angle X-ray scattering yields $A = 65.1$ Å^2 for DHPC at 48 °C. LAXS data provide the bending modulus, $K_C = 4.2 \times 10^{-13}$ erg, and the Hamaker parameter $H = 7.2 \times 10^{-14}$ erg for the van der Waals attractive interaction between neighboring bilayers. For the low temperature phases with ordered hydrocarbon chains, we confirm the transition from a tilted $L_{\beta'}$ gel phase to an untilted, interdigitated $L_\beta I$ phase as the sample hydrates at 20 °C. Our measurement of water permeability, $P_f = 0.022$ cm/s at 48 °C for fluid phase DHPC is slightly smaller than that of DPPC ($P_f = 0.027$ cm/s) at 50 °C, consistent with our triple slab theory of permeability.

1. Introduction

Ether lipids occur in biological systems primarily as plasmalogens, where the first carbon chain is attached to the glycerol backbone via an ether linkage, instead of the more common ester linkage as for the second carbon chain. Plasmalogens have been found in all mammalian tissues examined: nerve myelin can contain up to 52% plasmalogens of total phospholipids (O'Brien and Sampson, 1965). In ox heart, 45% of total phospholipids have ether linkages, primarily occurring in the mitochondria (Warner and Lands, 1961). About 15% of the phospholipids from human red blood cells are ether-linked lipids and this percentage is higher in white blood cells (Williams et al., 1966). Interestingly, ether lipids become elevated in tumor tissue by ~10% of the total lipid content (Snyder, 1972), which may signal macrophages to destroy them (Yamamoto and Ngwenya, 1987). In recent investigations of cancer treatment, synthetic alkyl phospholipids insert into the plasma membrane and kill tumor cells directly through apoptotic and non-apoptotic cell death and indirectly by causing interference in pathways that are critical for phospholipid survival (Mollinedo et al., 1997; Vink et al., 2007).

The effect of the ether linkage, compared to the ester linkage, on the structure and properties of lipid bilayers is of interest because it is a well localized chemical perturbation that affects physical properties. In order to focus solely on this specific linkage, many studies have compared dipalmitoylphosphatidylcholine (DPPC) which has two 16-carbon saturated chains attached to the glycerol backbone via ester linkages, with the model lipid, dihexadecylphosphatidylcholine (DHPC) which has ether linkages on both chains. One dramatic difference is that, whereas DPPC forms a conventional gel ($L_{\beta'}$) phase at room temperature, as DHPC hydrates it converts from a normal gel phase to a chain interdigitated ($L_\beta I$) phase (see Fig. 1) (Ruocco et al., 1985; Kim et al., 1987a; Laggner et al., 1987) and several hypotheses have been advanced for this phase transition (Laggner et al., 1987; Siminovitch et al., 1987; Hatanaka et al., 1997; Batenjany et al., 1997). The roles of headgroup hydration (Haas et al., 1990), headgroup orientation (Hauser, 1981), and membrane dipole potential and hydration force (Gawrisch et al., 1992) of DHPC have been investigated. Probes of DHPC have included changing pH (Furuike et al., 1999), changing hydrostatic pressure (Siminovitch et al., 1987) and binding to trehalose (Takahashi et al., 1997).

One of our main motivations for studying ether vs. ester linkages is to test a recent theory that proposes that the headgroup interfacial region is the major determinant of water permeability through membranes (Nagle et al., 2008). This theory was motivated by comparing structural and permeability data for five ester-linked phosphatidylcholines (Mathai et al., 2008). We now extend this database for this theory by changing the headgroup (our conven-

* Corresponding author at: Biological Physics Group, Department of Physics, Carnegie Mellon University, 5000 Forbes Avenue, Pittsburgh, PA 15213, USA. Tel.: +1 412 268 3174; fax: +1 412 681 0648.
E-mail address: stn@cmu.edu (S. Tristram-Nagle).

0009-3084/$ – see front matter © 2009 Elsevier Ireland Ltd. All rights reserved.
doi:10.1016/j.chemphyslip.2009.04.003

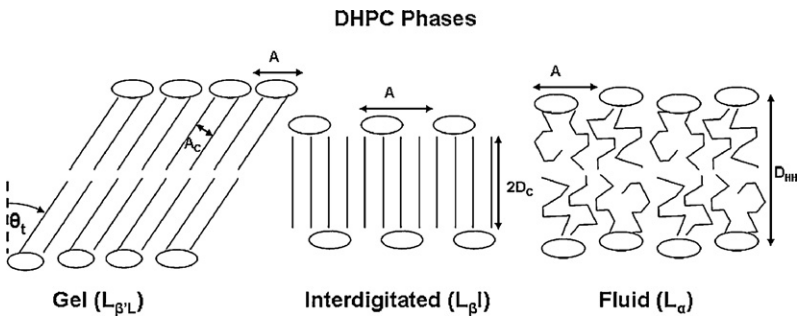

Fig. 1. DHPC phases: gel (partially dehydrated), interdigitated (fully hydrated) and fluid (fully hydrated, $T > 44\,^\circ$C). Important structural quantities such as chain tilt (θ_t), area/chain (A_C), area/lipid (A), hydrocarbon region thickness ($2D_C$) and head-to-head spacing (D_{HH}) are shown.

tion includes the phosphatidylcholine and the glycerol backbone as well as the ester vs. ether linkages in the headgroup) while keeping the chains (starting from the 2nd carbon) the same. Our structural work begins with conventional X-ray methods using both low angle lamellar scattering (LAXS) and wide angle scattering (WAXS) that confirm the room temperature $L_\beta I$ interdigitated structure and a partially dehydrated, $L_{\beta'}$ gel structure of DHPC in multilamellar samples. Enhanced analysis methods are used to refine these chain ordered structures. The fluid (L_α) phase structure of DHPC at 48 °C is obtained using modern analysis methods applied to LAXS diffuse X-ray scattering (Liu and Nagle, 2004) and to WAXS X-ray scattering (Mills et al., 2008). New results for the interactions between DHPC bilayers are also obtained. Both chain ordered and fluid phase structures are compared to our published structures of gel phase DPPC (Tristram-Nagle et al., 1993; Sun et al., 1996; Wiener et al., 1989) and fluid phase DPPC (Kučerka et al., 2006). The structural results are then compared to new measurements of water permeability through fluid phase DHPC bilayers.

2. Experimental

2.1. Materials and sample preparation

1,2-Dipalmitoyl-*sn*-glycero-3-phosphocholine (DPPC, Lot 160PC-267) and 1,2-dihexadecyl-*sn*-glycero-3-phosphocholine (DHPC, Lot 160DEPC-16 and 160DEPC-18) were purchased from Avanti Polar Lipids (Alabaster, AL) in the lyophilized form and used without further purification. Thin layer chromatography (TLC) using chloroform:methanol:7N NH_4OH (46:18:3, v/v/v) revealed < 0.1% lysolipid when stained with molybdic acid stain for DPPC and both lots of DHPC. HPLC grade organic solvents were purchased from Aldrich. Electrospray ionization mass spectroscopy verified that both lots of DHPC had the same molecular weight of (706 Da) and a purity > 99%. Optical rotatory dispersion (ORD) carried out by Dr. Steve Burgess at Avanti Polar Lipids detected ~20–30% of the D-isomer and ~70–80% L-isomer of DHPC in Lot 16, and ~100% L-isomer in Lot 18.

Four mg DHPC or DPPC was dissolved in 200 μl organic solvent (chloroform/methanol (3:1)) and then oriented onto 30 mm × 15 mm × 1 mm silicon wafers using the rock and roll technique (Tristram-Nagle, 2007), with the modification that for DHPC this technique was performed in an oven at 50 °C, since high temperature helped to orient this lipid. Hydration from water vapor was then carried out in a thick-walled hydration chamber (Kučerka et al., 2005) until the lamellar *D*-spacing was within 1–2 Å of its fully hydrated value.

Fully hydrated *D*-spacings were obtained from unoriented multilamellar vesicle (MLV) samples in excess water prepared by weighing 1–2 mg of dry lipid with 40 μl Milli-Q water and thoroughly mixed in small nalgene vials. These were vortexed and thermally cycled three times between 50 °C and −20 °C and loaded into 1 mm diameter glass capillaries. Large unilamellar vesicles (ULV) of ~60 nm diameter for structural studies were prepared in pure water by extrusion as described by Kučerka et al. (2005).

2.2. X-ray scattering experiments

X-ray data of oriented fluid phase DHPC at 48 °C were obtained at the Cornell High Energy Synchrotron Source (CHESS) using the G1 station on three separate trips on which the wavelength was set with a WB_4/C multilayer monochromater to 1.1797, 1.1808 and 1.2742 Å with a full width at half maximum of ±0.012 Å and the total beam intensity was $\sim 10^{11}$ photons/s. Beam widths were 0.2 mm; our preferred tall beam (0.6–1.0 mm vertical height) was unavailable on one trip when the beam had to be short (0.2 mm). The sample was ~10 μm thick along the normal to the ~2000 bilayers. Its dimension along the direction of the beam for LAXS was either narrow (5 mm) for use with the tall beam or wide (13 mm) for use with the short beam, and for WAXS the sample was narrow (4 mm). The flat samples were rotated from −3° to 7° in θ relative to the beam during the 30–60 s LAXS exposures and were X-rayed at fixed θ for the 10–20 s WAXS exposures. LAXS data from unoriented unilamellar vesicles (ULV) were also obtained as described by Kučerka et al. (2005) and exposure times were 60 s. For WAXS, $\theta = 0.2^\circ$ was used to first collect lipid scattering and then $\theta = -0.2^\circ$ was used to collect background chamber scattering that was subtracted from the lipid data (Mills et al., 2008). Data were collected by a Flicam CCD (Finger Lakes Instrumentation, Lima, NY) with a 1024 × 1024 pixel array and pixel size 69.78 μm/pixel. The sample-to-CCD distance was 400 mm for LAXS and 155 mm for WAXS. Temperature was controlled with a Neslab Controller (Portsmouth, NH) and monitored using a Cole-Parmer Thermistor Thermometer (Vernon Hills, IL).

MLV samples were X-rayed at 20 °C and 48–50 °C using a Rigaku RUH3R microfocus rotating anode (Woodlands, TX) equipped with a Xenocs FOX2D focusing collimation optic. Beam size was 1 mm × 1 mm and 20 min scans were collected using a Rigaku Mercury CCD detector with a pixel size of 68.0 μm/pixel; silver behenate ($D = 58.367$ Å) was used for calibration. A background capillary containing only Milli-Q water was subtracted from the lipid samples. Oriented gel phase data at 20 °C for both DPPC and DHPC (160DEPC-18) and WAXS data for DPPC at 50 °C were also collected using this X-ray setup. Temperature was controlled with a Julabo Controller (Allentown, PA) and monitored with a Cole-Parmer thermistor thermometer (Vernon Hills, IL).

2.3. Analysis of LAXS data from chain ordered phases

Intensities $I(h)$ of lamellar orders h were obtained from background subtracted discrete Bragg peaks. For oriented samples, an absorption correction was applied (Tristram-Nagle et al., 2002) and the usual Lorentz correction of q for oriented samples or q^2 for capillary samples was applied. Our detailed modeling analysis used a

Table 1
Summary of structural and interaction results for DHPC and DPPC.

	DHPC (int)	DHPC (gel)	DPPC (gel)	DHPC (fluid)	DPPC (fluid)
T (°C)	20	20	20	48	50
n_L (electrons)	394	394	406	394	406
ρ_{H_2O} (e/Å^3)	0.3337	0.3337	0.3337	0.3308	0.3300
V_L (Å^3)	1126[1]	1126	1144[2]	1223[1]	1229[1,2]
A (Å^2)	77.2	46.9	47.0[3–6]	65.1	64.3
D_{max} (Å)	47.8	60.5	63.4	67.9	66.7
D_{HH} (Å)	29.1	45.6	44.5[3]	38.2	37.8
$2D_C$ (Å)	20.3	34.6	34.6[6]	27.6	27.9
$D_{W'}$ (Å)	9.5	7.9	10.4	22.3	20.8
A_C (Å^2)	19.3	19.9	20.0[4]	–	–
K_C ($\times 10^{-13}$ erg)	–	–	–	4.2 ± 0.7	6.7 ± 0.7
$S_{X\text{-ray}}$	–	–	–	$0.36 \pm .04$	$0.41 \pm .02$
P_f ($\times 10^{-3}$ cm/s)	–	0.011 ± 0.007	0.012 ± 0.007	22 ± 6	27 ± 4
V_H (Å^3)	340	319	331	326	331
D_{H1} (Å)	4.39	5.49	4.95	5.3	4.95
V_C (Å^3)	786	806	813	897	897
λ_{fl} (Å)	–	–	–	8.4	4.3
P_{fl} ($\times 10^{-19}$ erg)	–	–	–	3.2	4.7
H ($\times 10^{-14}$ erg)	–	–	–	7.2	8.2

[1] Laggner et al. (1987), [2] Nagle and Wilkinson (1978), [3] Wiener et al. (1989), [4] Tristram-Nagle et al. (1993), [5] Sun et al. (1996) and [6] Sun et al. (1994).

2G hybrid electron density model (Wiener et al., 1989) as described previously (Tristram-Nagle et al., 2002). The 2G model consists of two pairs of headgroup Gaussians, a negative Gaussian for the methyl trough, a plateau for the water electron density and another plateau for the chain methylene electron density and a smooth, cosine bridging function to connect the two plateau regions. In the case of interdigitated DHPC, which is missing a central methyl trough, the second pair of 'headgroup' Gaussians was allowed to be negative to model the terminal methyl groups on the hydrocarbon chains. This program makes full use of non-LAXS data, such as the volume per lipid V_L and WAXS results listed in Table 1. The volume/lipid provides an important relation between the area A and the zeroth order form factor $F(0)$ (Nagle and Wiener, 1989):

$$AF(0) = 2(n_L - \rho_W V_L), \tag{1}$$

where n_L is the number of electrons/lipid and ρ_W is the electron density of water (see Table 1). Our modeling analysis also uses the chain tilt angle (θ_t) and the area A obtained from wide angle X-ray data.

2.4. Analysis of LAXS diffuse data from the fluid phase

The analysis of diffuse data has been described in previous publications (Lyatskaya et al., 2001; Liu and Nagle, 2004; Kučerka et al., 2005, 2006) and will be reviewed here only briefly. The scattering intensity for a stack of oriented bilayers is the product: $I(\mathbf{q}) = S(\mathbf{q})|F(q_z)|^2/q_z$, where $\mathbf{q} = (q_r, q_z)$, $S(\mathbf{q})$ is the structure interference factor, $F(q_z)$ is the bilayer form factor and q_z^{-1} is the usual low angle approximation to the Lorentz factor for narrow oriented samples and a tall beam for which all the sample remains in the beam for all relevant q. The Lorentz correction changes to q_z^{-2} when only a short beam was available and for which wide samples were used to ensure that the footprint of the beam on the sample was smaller than the sample for all relevant q. The first step of the analysis obtains the bilayer bending modulus (K_C), the compression modulus (B), and $|F(q_z)|^2/q_z$. The q_z axis for oriented $|F(q_z)|$ data was multiplied by 1.022 to correct for undulations (Nagle and Tristram-Nagle, 2000). In the second step, we used the H2 model (Klauda et al., 2006) to determine the electron density with the Fourier transform that best fits the experimental $|F(q_z)|$. In the H2 model the headgroups (phosphate and carbonyl/glycerol) and the methyl trough are modeled as Gaussians, while the water/choline density and methylene regions are modeled as error functions.

2.5. Analysis of fluid phase WAXS Data

WAXS emanates primarily from chain scattering that is affected by interchain distances and chain orientational order. The orientational order is obtained from the angular dependence $I(\phi)$ (where $\tan\phi = q_z/q_r$) of WAXS data from oriented samples which are analyzed following Mills et al. (2008). An X-ray order parameter:

$$S_{X\text{-ray}} = \frac{1}{2}(3\langle\cos^2\beta\rangle - 1) \tag{2}$$

provides a measure of the distribution of local tilt angles β.

2.6. Permeability Measurements

Water permeability P_f was measured as previously described (Lande et al., 1995; Mathai et al., 2008). First, ULV were prepared by weighing lipid (5 mg) into a glass vial and dissolving in 1:2 chloroform–methanol solution. The solvent was evaporated under nitrogen at 40 °C and residual solvent was removed under vacuum overnight. The dried lipid was hydrated in carboxyfluorescein (CF) buffer (100 mM NaCl, 50 mM sucrose, 10 mM of fluorescent probe 5–6 CF and 20 mM MOPS, pH 7.4) by cycling three times from 50 °C to −20 °C with vortexing. The lipid solution was then briefly probe sonicated for 30–60 s at a low setting of 5 mW (Virsonic 60, The Viritis Company Inc.). This lipid solution was extruded 21 times through a 100-nm nucleopore filter at 50 °C by using the Avanti mini-extruder assembly. Extravesicular CF was removed by passing the solution through a Sephadex PD-10 desalting column (Amersham) and the liposomes were collected in the void volume.

ULV in buffer were abruptly subjected to a 50% increase of external osmotic pressure in an Applied Photophysics (SX.18MV) stopped-flow device. The outflow of water decreases liposomal volume, which is measured by the self-quenching of entrapped carboxyfluorescein. All water permeability measurements were done within 120 min of ULV preparation at 20 °C (DHPC and DPPC), 48 °C (DHPC) and 50 °C (DHPC and DPPC). The sizes of the ULVs were obtained by dynamic light scattering using the Malvern nanoparticle sizer. The experimental osmotic water permeability coefficient, P_f, was obtained by finding the best comparison of the time constants obtained from single-exponential fits of the fluorescence decrease to those from a family of curves with varying P_f values that were generated using the water permeability equation and the measured ULV diameter.

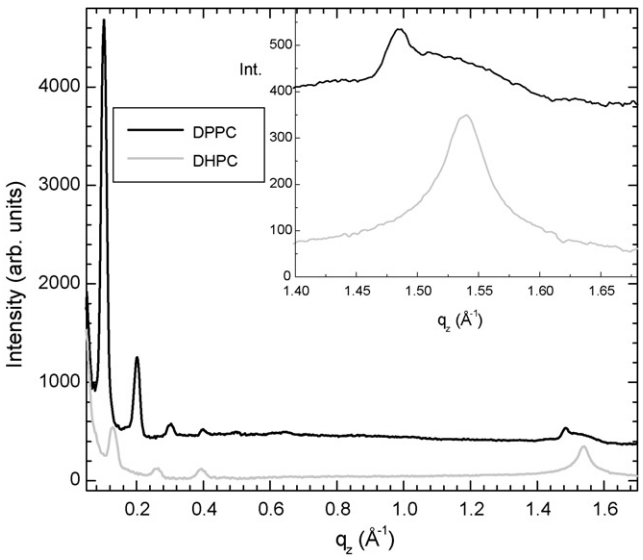

Fig. 2. LAXS and WAXS X-ray intensities of MLV of DPPC and DHPC in excess water in capillaries at 20 °C. The DPPC curves are displaced vertically.

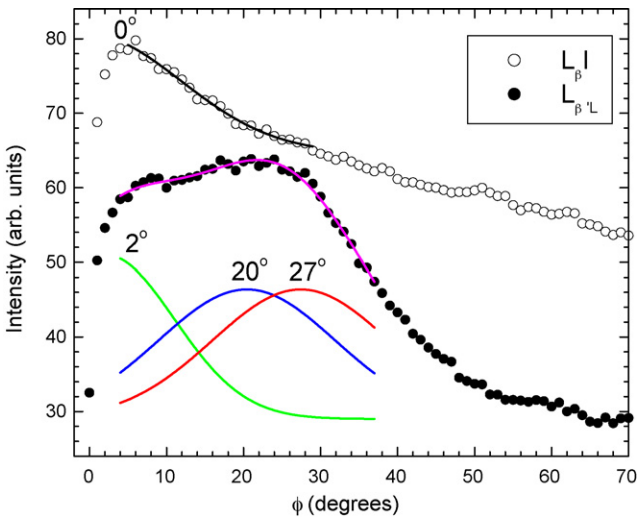

Fig. 4. $I(\phi)$ plot for DHPC in the $L_\beta I$ phase (open circles) with a Gaussian fit (black line), and for the drier, $L_{\beta' L}$ phase (solid circles). The $L_{\beta' L}$ intensity data were deconvoluted into three Gaussians, shown beneath the total intensity data, and the solid magenta line is their sum.

3. Results

3.1. Chain ordered phases

Fig. 2 shows X-ray diffraction data for fully hydrated MLV samples of both DHPC and DPPC at 20 °C in excess water in capillaries. The *D*-spacing results for these data, given in Table 1 as D_{max}, show that DHPC has a much smaller lamellar *D*-spacing than DPPC, consistent with an interdigitated $L_\beta I$ phase. Also evident in Fig. 2 is the WAXS (high *q* region), which is enlarged in the inset to Fig. 2. The DHPC WAXS shows a prominent, symmetrical peak, consistent with hexagonal packing of untilted rotamerically ordered chains with azimuthal disorder (Nagle, 1980), while a sharp peak with a broad shoulder in the DPPC WAXS is typical of orthorhombic packing of tilted chains (Tardieu et al., 1973; Sun et al., 1994).

Initially dry oriented samples were slowly hydrated through the vapor and the lamellar *D*-spacing of DHPC increased until it reached 60.5 Å for the data shown in Fig. 3A. Upon further hydration, the pattern changed dramatically as shown in Fig. 3B and the *D*-spacing decreased to 47.8 Å, which was the same value obtained for the fully hydrated *D*-spacing of unoriented MLV samples. The time for this phase transformation from gel to interdigitated phase ranged from less than measurable (~5 min) to as long as 2 h, depending upon the specific hydration conditions. As was mentioned in Section 2, well oriented samples of the ether-linked DHPC were more difficult to prepare than ester-linked lipids and larger mosaic spread, prominently visible in Fig. 3 (though only ~0.13° as determined by rocking scans, compared to <0.1° for ester-linked lipids), was present even after annealing at 50–60 °C in a humid environment.

Despite the relatively poorer orientation of these DHPC samples, WAXS data reveal considerably more structural information than WAXS from MLV samples. Fig. 3B suggests that there is an underlying single Bragg rod that has maximum intensity on the equator with tails extending $\sim L^{-1}$ to the positive and negative q_z directions, where *L* is the length of the hydrocarbon chains. This interpretation is substantiated in Fig. 4 which shows $I(\phi)$ plots. Since scattering intensity below 5° is decreased by absorbance of the sample and the silicon substrate, the maximum intensity at $q_r = 0$ is not actually observed, but its location at $q_r = 0$ is consistent with the Gaussian fit to the $I(\phi)$ data shown in Fig. 4. The relatively large width of this

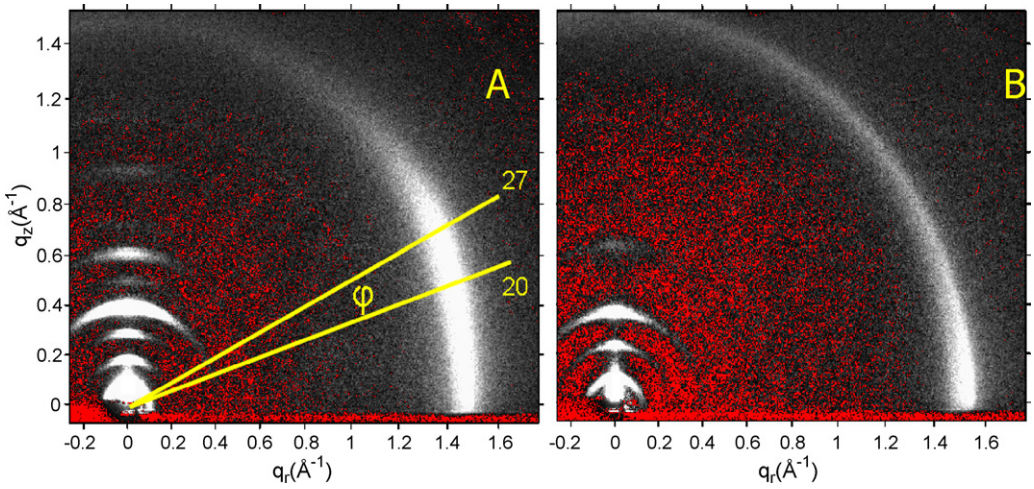

Fig. 3. CCD images of background subtracted scattering (LAXS at $q_r = 0$ Å^{-1} and WAXS near $q_r = 1.5$ Å^{-1}) at 20 °C from oriented samples of DHPC. The images are essentially grayscale with white showing high intensity and red pixels indicating small negative values. (A) Partially dry $L_{\beta' L}$ gel phase with a LAXS *D*-spacing of 60.5 Å. (B) Fully hydrated, interdigitated $L_\beta I$ phase with a LAXS *D*-spacing of 47.8 Å.

Gaussian compared to typical gel phase bilayers like DPPC is consistent with the thickness of the hydrocarbon region consisting of the length L of only one chain instead of two. These results are consistent with an $L_\beta I$ phase with the hydrocarbon chains perpendicular to the plane of the bilayer, i.e. chain tilt angle $\theta_t = 0$.

In contrast, the largest intensity for the drier $L_{\beta'L}$ phase in Fig. 3A occurs at a non-zero ϕ angle and this indicates that the chains are tilted by a non-zero angle θ_t. Although mosaicity makes a definitive interpretation impossible, Fig. 4 suggests that the $I(\phi)$ plot may be decomposed into three peaks, corresponding to the three Bragg rods that occur in an $L_{\beta'L}$ gel phase, adapting the notation of Smith et al. (1990), with chains tilted nearly toward nearest neighbor chains but with a deviation in the azimuthal angle of a few degrees. If so, then we estimate that the overall angle of the chain tilt θ_t is approximately 32° using the formulae in Tristram-Nagle et al. (1993, 2002).

Fig. 5 shows the chain packing d-spacing as a function of ϕ from the oriented WAXS data. For the $L_\beta I$ phase, the d-spacing of 4.09 Å for small ϕ does not vary significantly with increasing ϕ. Assuming a pattern of hexagonal chain packing, $d = 4.09$ Å gives a cross sectional area per hydrocarbon chain $A_C = 19.3$ Å^2 and then $\theta_t = 0$ gives an area A per lipid of $4A_C = 77.2$ Å^2. Also, the volume of the hydrocarbon region $V_C = 786$ Å^3 is obtained by multiplying $2A_C$ by the length of an all-trans chain (16×1.27 Å starting from the second carbon and using 2.54 Å for the terminal methyl). By contrast, at least two different d values are observed in the DHPC gel phase, which is expected for tilted chains in an orthorhombic packing. With our interpretation that this gel phase is an $L_{\beta'}L$ phase that is close to the usual $L_{\beta'}$ phase, we can approximate the larger $d = 4.23$ Å near $\phi = 0$ with d_{20} and the smaller $d = 4.12$ Å near $\phi = 30°$ with d_{11}. We then use the formula (Tristram-Nagle et al., 1993):

$$A_C = d_{20}d_{11}/\sqrt{1-(d_{11}/2d_{20})^2} \quad (3)$$

to obtain $A_C = 19.9$ Å^2 and $V_C = 806$ Å^3. We then obtain the area/lipid with $A = 2A_C/\cos\theta_t$. Then, using $\theta_t = 32°$ gives $A = 46.9$ Å^2 in the $L_{\beta'L}$ gel phase.

We obtained the intensities for nine orders of diffraction from oriented gel phase DHPC and took the square root of the Lorentz corrected intensities to give the relative values of the unsigned form factors. Our detailed analysis (Section 2.3) provided absolute form factors $|F(q_h)|$ shown in Fig. 6A for each order $h = 1$–9. Our

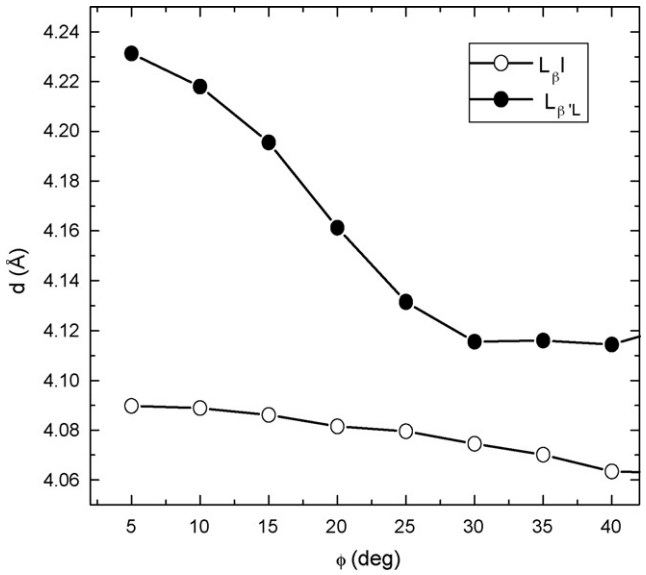

Fig. 5. WAXS D-spacing for DHPC at 20 °C as a function of φ, where $d = 2\Pi/q_{max}$ and q_{max} locates the maximum intensity along the radial with angle φ. The fully hydrated interdigitated $L_\beta I$ phase is shown with open circles and the drier $L_{\beta'L}$ gel phase is shown with solid circles.

analysis used $h = 0$ via Eq. (1) and the wide angle determination of A. Our refined analysis obtained the phase factors indicated by (±) in each lobe of the continuous Fourier transform $F(q_z)$ of the electron density profile. Even without the refined analysis, there is a sufficient range of D values (58.3–60.2 Å) that the phases can also be assigned in the conventional fashion (Kim et al., 1987a). Fig. 6B shows the Fourier reconstruction of the electron density profile from one sample with $D = 59.5$ Å. All samples gave very similar profiles with Fourier "wiggles" in the chain region due to a finite number of orders, while the headgroup peak is smooth with a weak shoulder toward the center of the bilayer. The electron density profile obtained from our refined modeling has a more physical, flat methylene region because that was imposed on the model. In addition to the main phosphate electron dense peak near ±23 Å, it also has secondary peaks near ±19 Å that arise from modeling the excess electron density of the glycerol backbone and the ether linkages.

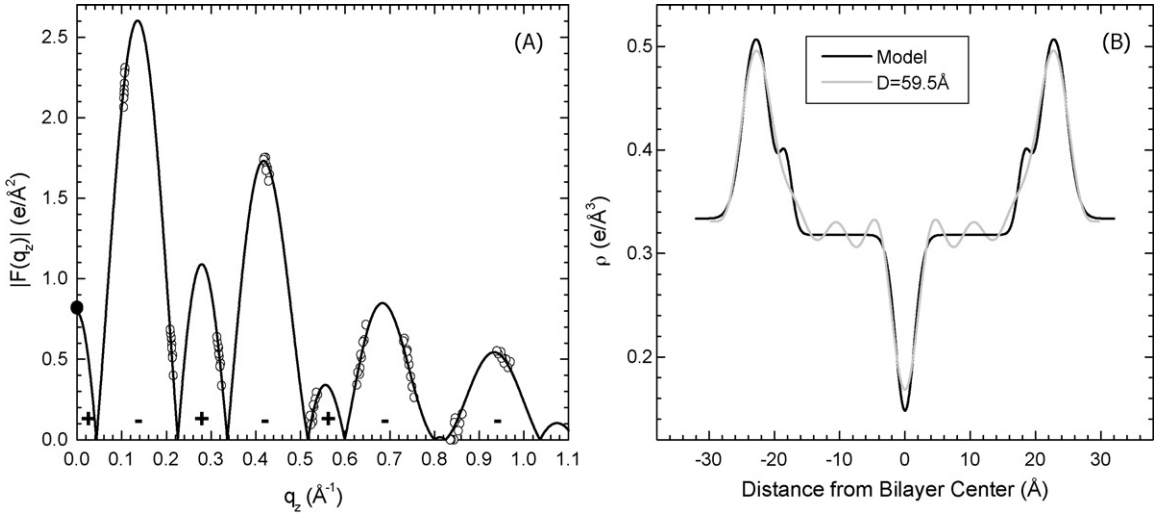

Fig. 6. (A) The symbols show absolute values of the form factors $|F(q_h)|$ for $h = 0$–9 from an oriented sample of DHPC $L_{\beta'L}$ phase for a range of $D = 58.3$–60.2 Å. The solid black line is the continuous Fourier transform of the electron density profile that emerges from our analysis. Phase factors (±) are indicated for each lobe. (B) Electron density profiles vs. distance z from the center of the bilayer. Our modeling analysis gives the smooth black solid line which gives the continuous transform $F(q_z)$ shown by the solid black line in (A). The wiggly gray line shows a Fourier reconstruction from the set of reflections obtained from the sample with $D = 59.5$ Å.

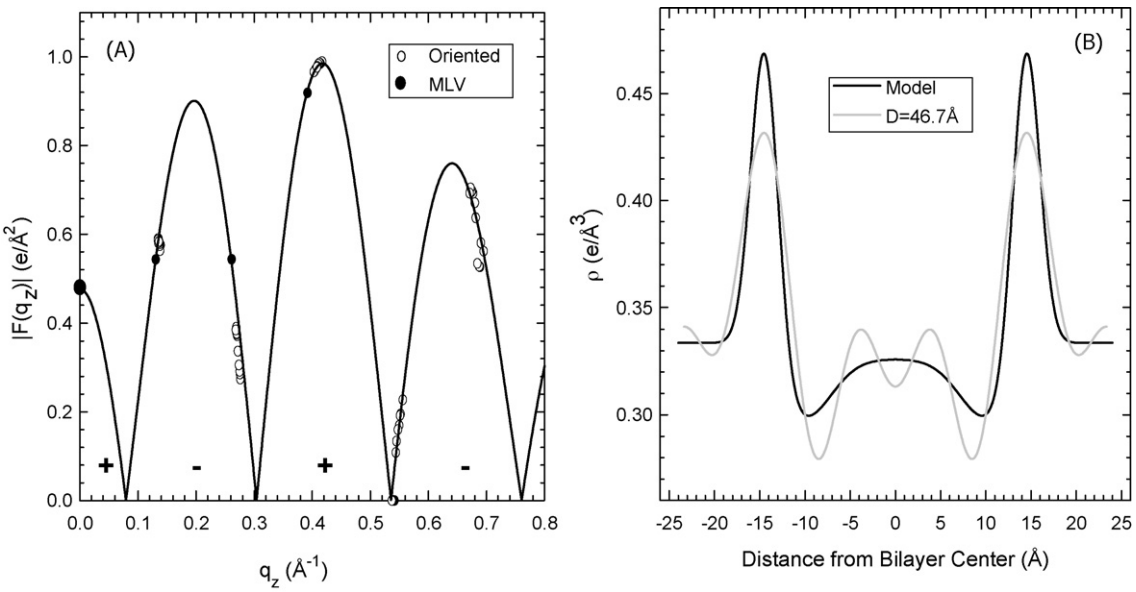

Fig. 7. (A) Absolute values of the form factors $|F(q_h)|$ for $h = 0$–5 from an oriented sample of DHPC $L_\beta I$ phase for a range of $D = 45.2$–46.8 Å (open circles) and $|F(q_h)|$ for $h = 0$–3 for unoriented MLV samples (solid circles). Continuous Fourier transform of the electron density profile that emerges from our analysis (solid black line). Phase factors (±) are indicated for each lobe. (B) Electron density profiles vs. distance z from the center of the bilayer. Our modeling analysis gives the smooth black solid line which gives the continuous transform $F(q_z)$ shown by the solid black line in (A). The wiggly gray line shows a Fourier reconstruction from the set of reflections obtained from the sample with $D = 46.7$ Å.

This unexpected feature was driven by the electron density model obtaining a better fit to the $|F(q_h)|$ data when the glycerol Gaussian has a narrow ~1 Å width. It cannot be justified solely by $|F(q_h)|$ data, which only have canonical resolution of 60 Å/h_{max}. Of course, the modeling analysis also includes additional information from WAXS and volume measurements, and the imposition of a model yields an extrapolation to an infinite number of orders. Nevertheless, caveats are in order, especially for this DHPC gel phase. First, the volume V_L could only be measured in the fully hydrated interdigitated phase and the gel phase volume is certainly different in view of the difference in wide angle spacings in Fig. 5. Second, the electron density in the methylene plateau inferred from WAXS was 0.312 e/Å^3 but, as also occurred in our study of the gel phase of DMPC (Tristram-Nagle et al., 2002), the fit to the data improved when this value was relaxed; the fit in Fig. 6 used 0.318 e/Å^3. Third, it was not possible to obtain θ_t accurately from WAXS due to the mosaic spread.

We obtained intensities for five orders of diffraction from oriented interdigitated phase DHPC, and three orders from a capillary sample in excess water (Fig. 7A, solid circles). We have frequently found that the ratio of the intensity of the $h = 1$ order to the intensity of higher orders is smaller in oriented samples than in MLV capillary samples, perhaps due to high reflectivity from the surface or extinction effects (Zachariasen, 1945). Because MLV samples are free of such artifacts, we have arbitrarily multiplied all the oriented $h = 1$ form factors by 2 so that they agree with the MLV data. (A similar factor was employed for the $h = 1$ form factors of the DHPC gel phase for which there were no MLV data. For both the gel and interdigitated phases, a very large uncertainty was assigned to the modified $h = 1$ intensities so they had negligible influence on fitting the analytical model to the $|F(q_h)|$ data.) The phase factors are easily assigned from Fig. 7A and agree with our modeling analysis which also assigns absolute values to $F(q_z)$. The Fourier reconstructions of the electron density profiles were similar for all D-spacings. As can be seen in Fig. 7B, the minimum at $z = 0$ is more likely to be a Fourier wiggle than a methyl trough, which instead is most likely to be located at the two deeper minima near ±8.5 Å, consistent with an interdigitated phase. This conclusion is strongly supported by our modeling analysis which gives the result in Fig. 7B that corresponds to the continuous Fourier transform in Fig. 7A. More detailed structural results are summarized in Table 1.

Curiously, however, as shown in Fig. 8, the form factors for ULVs of DHPC did not agree with the interdigitated form factor in Fig. 7A, but agreed much better with the gel phase form factor in Fig. 6A, indicating that the ULV ordered phase was a gel phase. This result was the same whether the solvent was pure water or buffer. It should be noted, however, that all measurements were done within 2 h of ULV preparation at high temperature and perhaps the interdigitated phase did not have time to form.

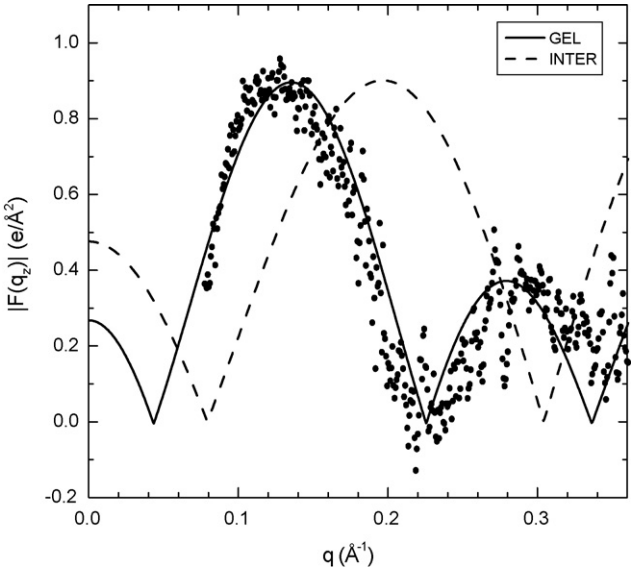

Fig. 8. Form factor data points from unilamellar vesicles of DHPC in water at 20 °C compared to continuous form factor transform of gel phase (solid line) and interdigitated phase (dashed line) results from multilamellar samples.

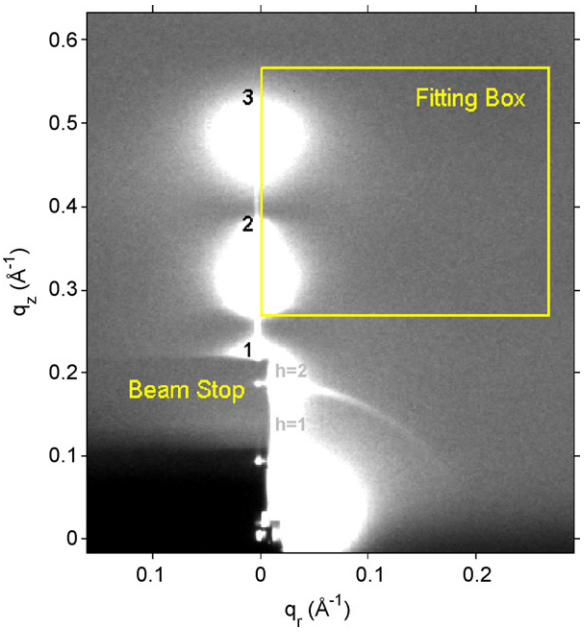

Fig. 9. CCD grayscale image of fluid phase LAXS from DHPC at 48 °C with higher intensity shown by white pixels and lower intensity by gray pixels. The beam and first two lamellar orders (h = 1 and 2) of the repeat spacing D = 66.1 Å are visible through a semi-transparent molybdenum beam stop that is located in the bottom left corner and has a thick part (black pixels) and a thinner part (dark gray pixels). The diffuse scattering lobes are numbered 1–3. The data used to determine K_C and B were contained in the yellow fitting box.

3.2. Fluid phase

Fig. 9 shows typical LAXS diffuse data for DHPC in the fluid phase. Results for the bending modulus, K_C, are shown in Fig. 10. K_C does not vary significantly with D, consistent with it being a property of single bilayers; the scatter in the values indicates the level of experimental uncertainty in the value of K_C. It may be noted that on the first CHESS trip with Lot 16 of DHPC, we were surprised to observe D-spacings for DHPC at 48 °C much higher than those for DPPC at 50 °C. (This temperature difference is insignificant; these temperatures were chosen since the volumes/lipid are known (Laggner et al., 1987; Nagle and Wilkinson, 1978).) Upon checking the purity with TLC we found that Lot 16 migrated as a single spot; additionally mass spec confirmed the correct molecular weight of 706 Da. Later, Avanti Polar Lipids carried out ORD and found contamination with up to 30% of the D-isomer in the usual L-isomer of DHPC. Avanti then supplied us with another sample of DHPC (Lot 18) with essentially 100% L-isomer. Lot 18 only swelled to 67 Å as shown in Fig. 10, and K_C was smaller than that of DPPC. These results for D suggest the interesting hypothesis that racemic mixtures may affect the interbilayer interactions and the results for K_C suggest that racemic mixtures may affect the stiffness of the bilayer. In Fig. 11 the B moduli are shown as a function of D-spacing. Lot 16 is included simply to show that a mixture of isomers produces quite different interbilayer behavior than the single, natural L-isomer. For the structural work in this paper, only Lot 18 DHPC was used.

As shown previously, there is no correlation between K_C and permeability through ester-linked bilayers (Mathai et al., 2008), so these results for K_C and B are of interest for fluctuations and interactions between bilayers rather than for water permeability. Following Pan et al. (2008), the fluctuation free energy $F_{fl} = (kT/2\pi)(B/K_C)^{1/2}$ was calculated as a function of D. The result (not shown) is well fit by $F_{fl} \sim \exp(-D/\lambda_{fl})$ which then implies that the fluctuation pressure $P_{fl} = F_{fl}/\lambda_{fl}$. At full hydration, the hydration pressure is negligible and the osmotic pressure is zero, so the fluctuation pressure was equated to the van der Waals attractive pressure to obtain the Hamaker parameter H. Calculating the van der Waals pressure requires the water spacing D_W (defined as $D - 2D_C - 18$ Å), where D_C is obtained from our subsequent structural determination. The numerical results are reported in Table 1.

After K_C and B were determined, the structure factor, $S(\mathbf{q})$, was calculated and the continuous $|F(q_z)|$ data on relative scales for oriented samples were obtained as described in Section 2. Fig. 12 shows some of our form factor data presented to indicate the level of experimental uncertainty. The solid magenta line is the Fourier transform of the electron density of the H2 model whose parameters were chosen to provide the best fit to the relative $F(q_z)$ results; this fitting procedure provides the absolute scale factor for $F(q_z)$. Also shown is $F(0)$ (solid circle) which was required to satisfy Eq. (1).

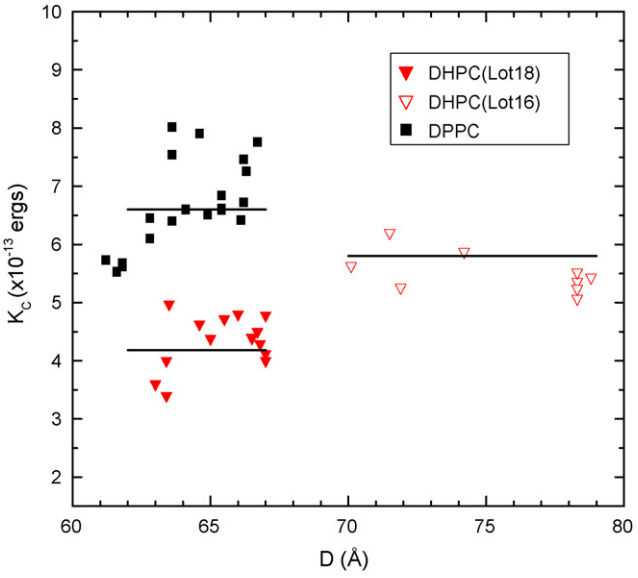

Fig. 10. Bending modulus, K_C, vs. D-spacing for two lots of DHPC at 48 °C: Lot 18 (solid triangles) and Lot 16 (open triangles). DPPC values (solid squares) at 50 °C are shown for comparison.

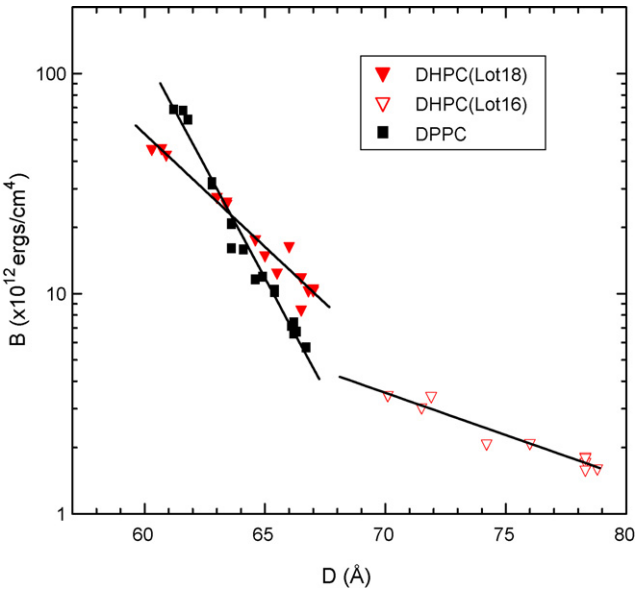

Fig. 11. B modulus vs. D-spacing for two lots of DHPC at 48 °C: Lot 18 (solid triangles) and Lot 16 (open triangles). DPPC values (solid squares) at 50 °C are shown for comparison.

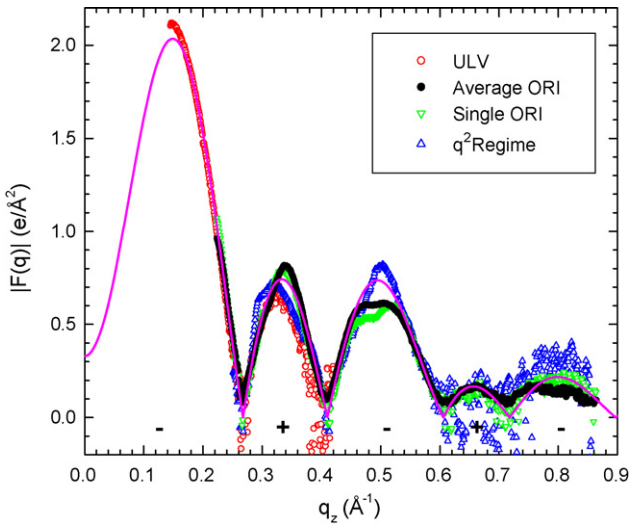

Fig. 12. Absolute continuous Fourier transforms of the electron density for DHPC fluid phase at 48 °C. The H2 model (solid magenta line) was fit to the ULV data (open red circles), oriented data averaged over 11 samples (open black circles), oriented data from a single sample (inverted open green triangles) and oriented data from a single sample using the q^2 (instead of q^1) data collection setup (open blue triangles).

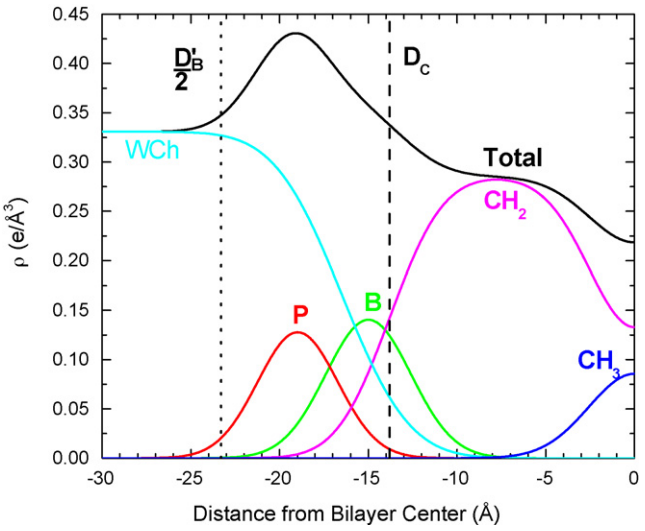

Fig. 13. Total electron density (black) for half a DHPC fluid phase bilayer at 48 °C obtained using the H2 model analysis. The contributions from the component groups are labeled P (phosphate group), B (glycerol backbone, ether linkage and first CH_2 on the hydrocarbon chains), CH_2 (remaining 14 methylenes on the chains), CH_3 (chain terminal methyls) and WCh (water plus choline group). D_C indicates the Gibbs dividing surface for the chain region and $D_{B'}$ is the steric thickness.

The electron density determined by the fit in Fig. 12 is shown in Fig. 13. The total electron density profile is shown as well as the component groups in the H2 model. Also shown in Fig. 13 is D_C, the Gibbs dividing surface for the hydrocarbon region, and $D_{B'}$, an estimate of the steric thickness. Fitting the H2 model requires the volume/headgroup, V_H. The volume of the hydrocarbon chain region V_C should be nearly the same for DPPC as for DHPC, so we used the same values as shown in Table 1, which then determined $V_H = 326$ Å^3 for DHPC from the V_L measurement. Our procedure usually requires using gel phase information for the distance D_{H1} from the phosphate peak to the hydrocarbon Gibbs dividing surface D_C. Surprisingly, when D_{H1} was allowed to be a free parameter, we obtained a good fit with D_{H1} close to the value deduced for the gel phase. Structural results are summarized in Table 1.

Fluid phase DHPC also produces WAXS diffuse scattering which results from chain–chain correlations described in detail by Mills et al. (2008). The WAXS d-spacing is centered near 4.6 Å, typical of fluid phase chain scattering. The rate of decay of the scattered intensity along ϕ, defined in Fig. 3, is related to the orientational order in the chains. Fig. 14 shows rather similar WAXS scattering for fluid phase DHPC and DPPC. However, there is a small difference in the $I(\phi)$ plots shown in Fig. 15. These data indicate that DHPC is more orientationally disordered than DPPC, and its orientational order parameter $S_{X\text{-ray}}$ is somewhat smaller as summarized in Table 1. Smaller $S_{X\text{-ray}}$ is correlated with larger area A (Mills et al., 2008), so this WAXS result is consistent with the larger A given by the LAXS result listed in Table 1.

3.3. Permeability results

The mean ULV diameters were 120 nm in DHPC and DPPC in the fluid phase and these decreased to 115 nm when the temperature was decreased to 20 °C. Water permeability (P_f) results are listed in Table 1 for both the fluid phase and the gel phase. As expected, P_f is much smaller in the gel phases than in the fluid phases. The fluid phase results for P_f reported in Table 1 are for DPPC at $T = 50$ °C (five separate samples) and for DHPC $T = 48$ °C (three separate samples); the latter temperature was chosen because that is where volume (Laggner et al., 1987) and other structural measurements were per-

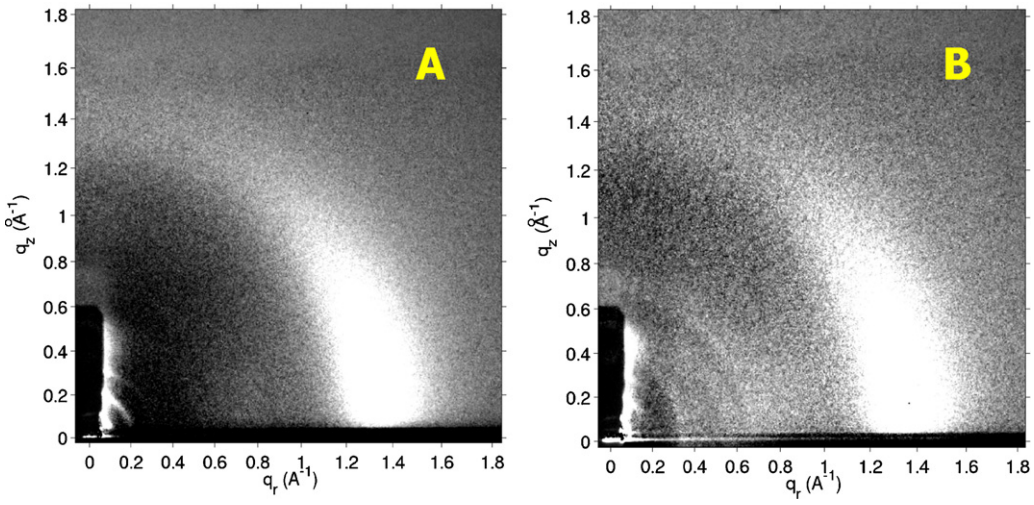

Fig. 14. (A) Fluid phase WAXS scattering for DPPC at 50 °C ($D = 61.7$ Å) and (B) DHPC at 48 °C ($D = 63.4$ Å).

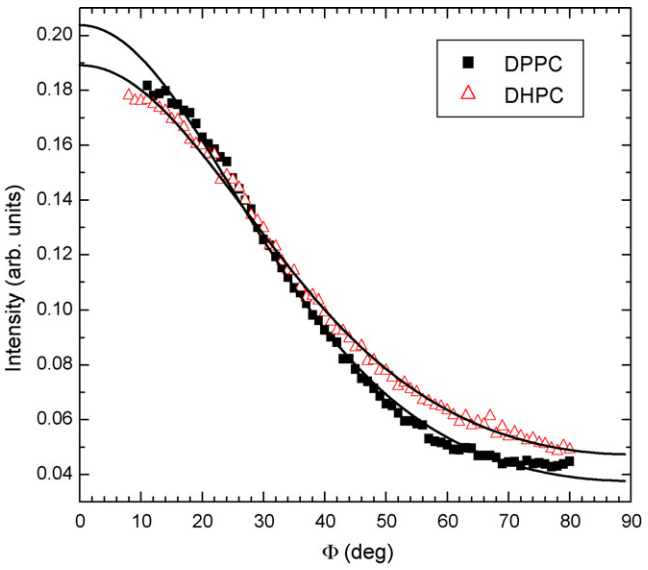

Fig. 15. I vs. φ plot for WAXS scattering of samples shown in Fig. 13: DPPC (solid squares) and DHPC (open triangles).

formed. The ratio $P_{f,DPPC}/P_{f,DHPC} = 1.2$ is >1, but this ratio could reflect the temperature difference. From a variety of P_f measurements as a function of temperature, we estimate that the mean value $P_{f,DPPC}/P_{f,DHPC} = 1.1$ at the same $T = 50\,^{\circ}C$. In an attempt to confirm this ratio, care was taken to prepare the DHPC and DPPC vesicles the same way and then at $T = 50\,^{\circ}C$, $P_f = 0.035$ cm/s was obtained for DPPC and $P_f = 0.033$ cm/s was obtained for DHPC, again giving $P_{f,DPPC}/P_{f,DHPC} = 1.1$. Despite the consistency with the initial data, the uncertainties in this ratio are at least as large as 0.2. As was noted by Mathai et al. (2008), literature values for water permeability vary considerably from one lab to another. Although ratios of P_f for different bilayers are generally more robust than the absolute values, our $P_{f,DPPC}/P_{f,DHPC}$ for the fluid phase at $T = 50\,^{\circ}C$ differs considerably from a literature value of $P_{f,DPPC}/P_{f,DHPC} \approx 15$ at $70\,^{\circ}C$ using a glucose-induced osmotic shock change in vesicle size measured with light scattering (Jansen and Blume, 1995); this latter study also reported a ratio of 4.3 in the gel phase that is considerably larger than our ratio that is also close to 1 from Table 1. Since the ratio should not depend strongly upon temperature and since their sample preparation of ULV was similar to ours, these differences are unexplained.

4. Discussion

4.1. Test of theories of water permeability in the fluid phase

The simplest theory of water permeability regards the permeability barrier as the hydrocarbon region, which it treats as a single slab, and the textbook formula for permeability is $P_f = K_{partition} D_{diffusion}/2D_C$. Our structural results indicate that the hydrocarbon thickness $2D_C$ is slightly smaller in the fluid phase for DHPC than for DPPC. Also, our $S_{X\text{-}ray}$ order parameter is smaller for DHPC indicating that its hydrocarbon region of DHPC is slightly more disordered, and this would be consistent with larger, not smaller values of $K_{partition}$ and $D_{diffusion}$. Although the uncertainties in our measured values for P_f would permit the textbook formula to be consistent, our most probable measured ratio $P_f(DPPC)/P_f(DHPC) = 1.1$ is slightly >1 rather than <1; this does not favor the single slab model.

Our recently developed theory of water permeability (Nagle et al., 2008) invokes a model with a central hydrocarbon slab flanked by two headgroup slabs so P_f is given by the formula for resistances in series, $1/P_f = 2/P_H + 1/P_C$, where P_H is the permeability of each headgroup slab and P_C is the permeability of the hydrocarbon slab. The strong correlation of the permeability data obtained for ester-linked lipids with the area/lipid A suggested that the rate limiting step for water permeability is due to the headgroup slabs ($P_H < P_C$). Neglecting the secondary influence of the hydrocarbon slab, P_f is mostly due to P_H which was predicted to be proportional to $(K_{partition} D_{head}/d_{head})(A - A_0)/A$, where A is the measured surface area per lipid, A_0 is a blocked area that is basically the gel phase area A_{gel} plus an additional steric area due to the size of the permeating water molecule, $K_{partition}$ is again the partition coefficient in the hydrocarbon region, d_{head} is the thickness of the headgroup slab and D_{head} is the diffusion coefficient of water in the unobstructed portion of the headgroup region (Nagle et al., 2008). Our structural results suggest that there is little difference in d_{head} between DHPC and DPPC in the fluid phase, and the similarities in the hydrocarbon region suggest that $K_{partition}$ should be nearly the same at the same temperature. The structure of DHPC in Table 1 was determined at $48\,^{\circ}C$. To compare to previous structure of DPPC at $50\,^{\circ}C$ we use $\alpha_A = (dA/dT)/A \sim 0.003/^{\circ}C$ to estimate $A = 65.5\,Å^2$ for DHPC at $50\,^{\circ}C$. Therefore, this somewhat larger value of A for DHPC means that A_0 must be larger or D_{head} must be smaller for DHPC for the three slab theory to be valid. An NMR result that water is slightly more ordered in DHPC than in DPPC (Gawrisch et al., 1992) is consistent with a smaller D_{head}. While quite plausible, our X-ray structural study can offer no additional evidence to support this interpretation, so we turn to considering structural evidence that A_0 may be larger for DHPC than for DPPC. For ester-linked PC lipids the data suggested that $A_0 \sim 53\,Å^2$ (Nagle et al., 2008). If we ignore any difference in D_{head}, our measured permeability ratio of 1.06 for DPPC vs. DHPC would require $A_0 \sim 54.8\,Å^2$ for DHPC.

4.2. Structure of chain ordered phases

Earlier X-ray measurements on MLV samples revealed that fully hydrated DHPC near room temperature forms a fully interdigitated phase (Ruocco et al., 1985). A subsequent study reported quantitative results for the lamellar D-spacing ($D = 47.0\,Å$), the headgroup thickness ($D_{HH} = 30\,Å$), and the area ($A_{interdigitated} = 77\,Å^2$) (Kim et al., 1987a), with which our corresponding results in Table 1 agree quite well. Their continuous $F(q)$ transform has its maximum in the first lobe instead of the second lobe in Fig. 7, but the electron density profiles from the Fourier reconstructions are quite similar. Our modeling in real space fits the $|F(q)|$ reciprocal space data very well in Fig. 7. The resulting electron density model confirms that the minima in the Fourier reconstructions are the locations of the electron sparse terminal methyl groups and not just Fourier wiggles. Because we used oriented samples, our WAXS results in Fig. 4 provide direct evidence for the absence of chain tilt.

While our oriented samples were hydrating, we also observed the gel phase that was previously obtained with limited water content. The pattern of our $|F(q)|$ data agree quite well with Kim et al. (1987a); we extended their data from $0.75\,Å^{-1}$ to nearly $1.0\,Å^{-1}$, which added an extra lobe in Fig. 6A. Nevertheless, their $D_{HH} = 46\,Å$ agrees well with ours in Table 1. Our higher resolution more clearly shows constant electron density in the methylenic region in the Fourier reconstruction of the electron density in Fig. 6B. Our electron density modeling gives rather narrowly defined spatial features suggesting that this gel phase is well ordered.

Our area for the DHPC gel phase was computed using $A = 2A_C/\cos\theta_t$. While our value of A_C from WAXS is obtained straightforwardly (Eq. (3)), the value of θ_t that we obtain from Fig. 4 requires some interpretation. We suggest that the drier gel phase could be a phase that was notated as the $L_\beta L$ phase (Smith et al., 1990). We modify this notation to $L_{\beta'}L$, where the added prime is the conventional notation for tilted chains. Smith et al. (1990) empha-

sized that the conventional description of gel phases is incomplete because it does not include the azimuthal direction of the chain tilt and this distinction is notated by the final subscripted letter. The best-known gel phase is the one for DPPC in which the direction of tilt of each chain is toward a nearest neighboring chain; we notate this as $L_{\beta' I}$, where the placement of the I as a subscript reminds one not to mistake it for the interdigitated $L_\beta I$ phase. There is also the $L_{\beta' F}$ phase where the direction of chain tilt is directly between nearest neighboring chains; this phase has two WAXS peaks above the equator in the first quadrant in q space instead of one peak off the equator and one on the equator as in the $L_{\beta' I}$ phase. The $L_{\beta' L}$ phase has the direction of chain tilt at any of the angles between those of the $L_{\beta' I}$ and $L_{\beta' F}$ phases; it has three WAXS peaks off the equator. Our analysis shown in Fig. 4 is consistent with the gel state of DHPC being an $L_{\beta' L}$ phase that has an azimuthal direction of tilt angle closer to the $L_{\beta' I}$ state than to the $L_{\beta' F}$ state and we estimate that the chains have an overall $\theta_t \sim 32^\circ$, close to that of DPPC (Tristram-Nagle et al., 1993; Sun et al., 1996). However, we do not attach high accuracy to our estimate of θ_t or A. Because θ_t and A generally increase with hydration in the gel phase (Tristram-Nagle et al., 2002), values for this partially hydrated phase would only be expected to provide a basis for a lower bound to the value of A_0 that is central to discussion of the permeability theory. It may also be noted that application of the gravimetric Luzzati method, which usually gives values of A that are too large (Nagle and Tristram-Nagle, 2000), gave $A = 48$ Å^2 (Kim et al., 1987a).

The standard argument for discussing why a lipid membrane would become interdigitated rather than have an ordinary gel phase involves the competition between two free energy terms (Hatanaka et al., 1997). One term involves van der Waals interactions between chains, which is more favorable for a phase with smaller A_C. Our results for A_C in Table 1 show that this favors the interdigitated phase compared to the gel phase of DHPC. The other term is the hydrophobic free energy which is generally unfavorable for the interdigitated phase because it has more exposed hydrocarbon than a gel phase. However, as the headgroup area becomes larger, there is less exposed hydrocarbon in an interdigitated structure (Fig. 1), so the difference in this term brought about by a larger headgroup area helps make the $L_\beta I$ phase more favorable. To these two terms we would also add a third term that penalizes larger tilt angles (Tristram-Nagle et al., 1993; Sun et al., 1996) which would be required by a larger headgroup area A_{gel}. The structural result that fully hydrated DHPC is in the interdigitated phase is therefore consistent with a larger A_0 than in DPPC.

It is noteworthy, however, that the argument in the preceding paragraph does not explain our result that ULV of DHPC do not form the interdigitated phase, at least when the solvent is buffered. It is especially counterintuitive that multilamellar systems convert from gel to interdigitated phases upon increased hydration while the ultimately hydrated ULV form gel phase instead of interdigitated phase. Apparently, the weak interbilayer interactions in multilamellar samples suffice to tip the already delicate balance between gel and interdigitated phases.

4.3. Structure of fluid phase

The most robust quantity that can be obtained from our X-ray method is D_{HH}, the head to head distance between the maxima in the electron density profile. Our value 38.2 Å in Table 1 compares well with the value 38 Å reported by Kim et al. (1987a), but their value was obtained at $T = 65\,^\circ$C (which decreases D_{HH}) and at low hydration (which increases D_{HH}). A subsequent paper showed $D_{HH} = 46$ Å at $T = 50\,^\circ$C (Fig. 4 in Kim et al., 1987b). They also reported $A = 61$ Å^2 at $T = 65\,^\circ$C using the gravimetric method (Kim et al., 1987a); this value is significantly smaller than recent values of A for DPPC (Kučerka et al., 2006, 2008). While this difference would directly help explain the smaller permeability of DHPC, we will argue for the larger value we give in Table 1. The simplest argument is that the orientational order parameter $S_{X\text{-ray}}$ obtained from Fig. 15 is slightly smaller for DHPC and this implies that the thickness $2D_C$ of the hydrocarbon region should be smaller. Because the hydrocarbon volume V_C in Table 1 should be nearly the same, the relation $A = V_C/D_C$ suggests that DHPC has an area greater than DPPC. Support for A for DHPC being larger than for DPPC also comes from simulations performed under similar conditions by Alex deVries.

Our standard method for obtaining A for fluid phases requires information in addition to LAXS data. The outside information used in this paper for DHPC was that we took the volume V_C of the hydrocarbon region to be the same for DPPC and DHPC. Together with the measured volume V_L of the lipid, this determines the volume V_H of the headgroup to be quite similar to DPPC in Table 1; this would appear to be reasonable because the replacement of a C=O group with CH_2 would not likely change the volume significantly. Our standard method also inputs the quantity $D_{H1} = D_{HH}/2 - D_C$ from the gel phase, but this was not necessary for DHPC. Our output value of D_{H1} is close to the value we obtained for the gel phase of DHPC but significantly larger than the even better determined value for the interdigitated phase. However, the smaller value for the interdigitated phase is likely due to the sliding of the headgroups on opposite sides towards the center of the bilayer so that the terminal methyls overlap with the glycerol groups, thereby shortening D_{HH} without changing the average hydrocarbon thickness $2D_C$. Such an option is unavailable in proper bilayers, so D_{H1} for the interdigitated phase is probably irrelevant for the fluid phase. It may be noted that other studies have indicated little change in the headgroup structure in ether-linked lipids. An MD simulation comparing ester and ether-linked diphytanoyl PC found that the distance from the bilayer center to each atom in the headgroup region was identical within error for both ether and ester linkages; the only difference was slightly more sharply ordered P–N and C–C vectors for the ether-linked headgroup (Shinoda et al., 2004). Hauser (1981) used NMR to show that the motionally averaged conformation of the glycerophosphocholine group is similar in ether and ester-linked phospholipids, indicating no significant effect on the average conformation and segmental motion of the polar group. This was based on ^{1}H spin–spin coupling constants and also ^{31}P NMR which indicate free rotation about the C2–C3 glycerol bond both above and below the main phase transition and the proton decoupled ^{31}P NMR

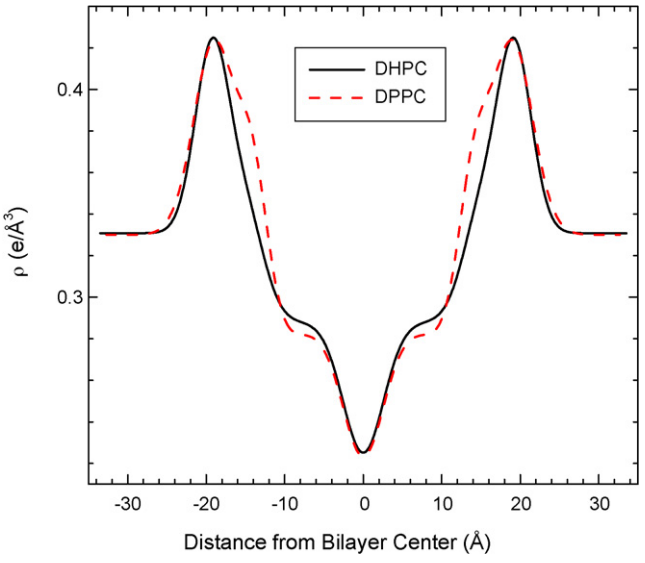

Fig. 16. Comparison of electron density profiles for fluid phase DHPC (solid line) and DPPC (dashed line, from Kučerka et al., 2006).

spectra of unsonicated aqueous dispersions of DPPC and DHPC were virtually identical. It is unclear, however, whether these studies would be sensitive to the small differences in D_{H1} that we obtain.

Comparison of the continuous transform obtained from this constrained modeling agrees quite well with our LAXS data as seen in Fig. 12. Although there is little difference in the physical parameters for DHPC and DPPC in Table 1, Fig. 16 shows a clear difference in the electron density profile in the region from 12 to 18 Å caused by replacement of a carbonyl group with 14 electrons in DPPC by a methylene group with only 8 electrons in DHPC.

5. Conclusions

Our results in Table 1 show rather modest differences in the fluid phase structures of DHPC vs. DPPC bilayers. The greatest differences between bilayers of ether and ester-linked lipids appear to be the membrane dipole potential (Gawrisch et al., 1992) which is only half as large in the fluid phase of DHPC as in DPPC, and the different electron density in Fig. 16. Both these differences are consistent with the chemical replacement of the strongly dipolar C=O group with a CH_2 group that has less electron density. On the other hand, there is a large difference in the ordered chain phases, namely, the well-established appearance (Kim et al., 1987a) of the interdigitated phase in multilamellar samples of fully hydrated DHPC. An interdigitated phase would be consistent with a larger "null" area A_0 for DHPC that plays a role in a recent theory for water permeability that invokes physical blockage in the headgroup region. However, it is at least as likely that the chemical effect of the ether linkage on the local diffusion constant D_{head} would play the major role in that theory. More stringent testing of the permeability theory for ether-linked lipids would require a parallel study to the one we have performed for ester-linked phosphatidylcholine bilayers (Mathai et al., 2008) where five lipids with differing chain lengths and degrees of saturation provided significantly different areas A per lipid.

Acknowledgments

We would like to thank Rob Chan and David Lenkner for help with the fluid phase data collection and analysis, Dong Joo Kim for help with ULV data analysis, Dr. Norbert Kučerka for help with the ULV data collection, Dr. Thalia Mills for help with the wide angle analysis, and Dr. Alex deVries for sharing his simulation results before publication. This research was supported by NIH Grant No. GM 44976 (PI-JFN) and DK 43955 (PI-MZ). S.D.G. and D.D.G. were funded through Howard Hughes Medical Institute undergraduate research. X-ray scattering data were taken at the Cornell High Energy Synchrotron Source (CHESS), which is supported by the National Science Foundation and the National Institutes of Health/National Institute of General Medical Sciences under National Science Foundation award DMR-0225180.

References

Batenjany, M.M., O'Leary, T.J., Levin, I.W., Mason, J.T., 1997. Packing characteristics of two-component bilayers composed of ester- and ether-linked phospholipids. Biophys. J. 72, 1695–1700.

Furuike, S., Levandy, V.G., Li, S.J., Yamazaki, M., 1999. Low pH induces an interdigitated gel to bilayer phase transition in dihexadecylphosphatidylcholine membrane. Biophys. J. 77, 2015–2023.

Gawrisch, K., Ruston, D., Zimmerberg, J., Parsegian, A., Rand, P.R., Fuller, N., 1992. Membrane dipole potentials, hydration forces, and ordering of water are membrane surfaces. Biophys. J. 61, 1213–1223.

Haas, N.S., Sripada, P.K., Shipley, G.G., 1990. Effect of chain-linkage on the structure of phosphatidylcholine bilayers. Biophys. J. 57, 117–124.

Hatanaka, Y., Kinoshita, K., Yamazaki, M., 1997. Osmotic stress induces a phase transition from interdigitated gel phase to bilayer gel phase in multilamellar vesicles of dihexadecylphosphatidylcholine. Biophys. Chem. 65, 229–233.

Hauser, H., 1981. The polar group conformation of 1,2-dialkyl phosphatidylcholines, an NMR study. Biochim. Biophys. Acta 646, 203–210.

Jansen, M., Blume, A., 1995. A comparative study of diffusive and osmotic water permeation across bilayers composed of phospholipids with different headgroups and fatty acyl chains. Biophys. J. 68, 997–1008.

Kim, J.T., Mattai, J., Shipley, G.G., 1987a. Gel phase polymorphism in ether-linked dihexadecylphosphatidylcholine bilayers. Biochemistry 26, 6592–6598.

Kim, J.T., Mattai, J., Shipley, G.G., 1987b. Bilayer interactions of ether- and ester-linked phospholipids: dihexadecyl- and dipalmitoylphosphatidylcholines. Biochemistry 26, 6599–6603.

Klauda, J.B., Kučerka, N., Brooks, B.R., Pastor, R.W., Nagle, J.F., 2006. Simulation-based methods for interpreting X-ray data from lipid bilayers. Biophys. J. 90, 2796–2807.

Kučerka, N., Liu, Y., Chu, N., Petrache, H.I., Tristram-Nagle, S., Nagle, J.F., 2005. Structure of fully hydrated fluid phase DMPC and DLPCl lipid bilayers using X-ray scattering from oriented multilamellar arrays and from unilamellar vesicles. Biophys. J. 88, 2626–2637.

Kučerka, N., Tristram-Nagle, S., Nagle, J.F., 2006. Closer look at structure of fully hydrated fluid phase DPPC bilayers. Biophys. J.: Biophys. Lett. 90, L83–85.

Kučerka, N., Nagle, J.F., Sachs, J.N., Feller, S., Pencer, J., Jackson, A.J., Katsaras, J., 2008. Lipid bilayer structure determined by the simultaneous analysis of neutron and X-ray scattering data. Biophys. J. 95, 2356–2367.

Laggner, P., Lohner, K., Degovics, G., Müller, K., Schuster, A., 1987. Structure and thermodynamics of the dihexadecylphosphatidylcholine–water system. Chem. Phys. Lipids 44, 31–60.

Lande, M.B., Donovan, J.M., Zeidel, M.L., 1995. The relationship between membrane fluidity and permeabilities to water, solutes, ammonia, and protons. J. Gen. Physiol. 106, 67–84.

Liu, Y., Nagle, J.F., 2004. Diffuse scattering provides material parameters and electron density profiles of biomembranes. Phys. Rev. E 69, 040901(R) (Rapid Communications).

Lyatskaya, Y., Liu, Y., Tristram-Nagle, S., Katsaras, J., Nagle, J.F., 2001. Method for obtaining structure and interactions from oriented lipid bilayers. Phys. Rev. E 63, 0119071–0119079.

Mathai, J.C., Tristram-Nagle, S., Nagle, J.F., Zeidel, M.L., 2008. Structural determinants of water permeability through the lipid membrane. J. Gen. Physiol. 131, 69–76.

Mills, T.T., Toombes, G.E.S., Tristram-Nagle, S., Smilgies, D.-M., Feigenson, G.W., Nagle, J.F., 2008. Order parameters and areas in fluid-phase oriented lipid membranes using wide angle X-ray scattering. Biophys. J. 95, 669–681.

Mollinedo, F., Fernández-Luna, J.L., Gajate, C., Martín-Martín, B., Benito, A., Martínez-Dalmau, R., Modolell, M., 1997. Selective induction of apoptosis in cancer cells by the ether lipid ET-18-OCH3 (Edelfosine): molecular structure requirements, cellular uptake, and protection by Bcl-2 and Bcl-X(L). Cancer Res. 57, 1320–1328.

Nagle, J.F., Mathai, J.C., Zeidel, M.L., Tristram-Nagle, S., 2008. Theory of passive permeability through lipid bilayers. J. Gen. Physiol. 131, 77–85.

Nagle, J.F., Tristram-Nagle, S., 2000. Structure of lipid bilayers. Biochim. Biophys. Acta 1469, 159–195.

Nagle, J.F., 1980. Theory of the main lipid bilayer phase transition. Annu. Rev. Phys. Chem. 31, 157–195.

Nagle, J.F., Wiener, M.C., 1989. Relations for lipid bilayers: connection of electron density profiles to their structural quantities. Biophys. J. 55, 309–313.

Nagle, J.F., Wilkinson, D.A., 1978. Lecithin bilayers. Density measurement and molecular interactions. Biophys. J. 23, 159–175.

O'Brien, J.S., Sampson, E.L., 1965. Lipid composition of normal human brain—gray matter, white matter and myelin. J. Lipid Res. 6, 537–544.

Pan, J., Mills, T.T., Tristram-Nagle, S., Nagle, J.F., 2008. Temperature dependence of structure, bending rigidity and bilayer interactions of DOPC bilayers. Biophys. J. 94, 117–124.

Ruocco, M.J., Siminovitch, D.J., Griffin, R.G., 1985. Comparative study of the gel phases of ether- and ester-linked phosphatidylcholines. Biochemistry 24, 2406–2411.

Siminovitch, D.J., Wong, P.T.T., Mantsch, H.H., 1987. High-pressure infrared spectroscopy of ether and ester-linked phosphatidylcholine aqueous dispersions. Biophys. J. 51, 465–473.

Shinoda, K., Shinoda, W., Baba, T., Mikami, M., 2004. Comparative molecular dynamics study of ether- and ester-linked phospholipid bilayers. J. Chem. Phys. 121, 9648–9654.

Smith, G.S., Sirota, E.B., Safinya, C.R., Plano, R.J., Clark, N.A., 1990. X-ray structural studies of freely suspended ordered hydrated DMPC multimembrane films. J. Chem. Phys. 92, 4519–4529.

Snyder, F., 1972. Ether-linked lipids and fatty alcohol precursors in neoplasms. In: Snyder, F. (Ed.), Ether Lipids Chemistry and Biology. Academic Press, New York, pp. 273–295.

Sun, W.-J., Suter, R.M., Knewtson, M.A., Worthington, C.R., Tristram-Nagle, S., Zhang, R., Nagle, J.F., 1994. Order and disorder in fully hydrated unoriented bilayers of gel phase dipalmitoylphosphatidylcholine. Phys. Rev. E, 4665–4676.

Sun, W.-J., Tristram-Nagle, S., Suter, R.M., Nagle, J.F., 1996. Structure of gel phase saturated lecithin bilayers: temperature and chain length dependence. Biophys. J. 71, 885–891.

Takahashi, H., Ohmae, H., Hatta, I., 1997. Trehalose-induced destabilization of interdigitated gel phase in dihexadecylphosphatidylcholine. Biophys. J. 73, 3030–3038.

Tardieu, A., Luzzati, V., Reman, F.C., 1973. Structure and polymorphism of the hydrocarbon chains of lipids: a study of lecithin–water phases. J. Mol. Biol. 75, 711–733.

Tristram-Nagle, S., 2007. Preparation of oriented, fully hydrated lipid samples for structure determination using X-ray scattering. In: Dopico, A. (Ed.), Methods in

Molecular Biology 400 (Methods in Membrane Lipids). Humana Press, Totowa, NJ, pp. 63–75.
Tristram-Nagle, S., Liu, Y., Legleiter, J., Nagle, J.F., 2002. Structure of gel phase DMPC determined by X-ray diffraction. Biophys. J. 83, 3324–3335.
Tristram-Nagle, S., Zhang, R., Suter, R.M., Worthington, C.R., Sun, W.-J., Nagle, J.F., 1993. Measurement of chain tilt angle in fully hydrated bilayers of gel phase lecithins. Biophys. J. 64, 1097–1109.
Warner, H.R., Lands, W.E.M., 1961. Metabolism of plasmalogen—enzymatic hydrolysis of vinyl ether. J. Biol. Chem. 236, 2404–2409.
Wiener, M.C., Suter, R.M., Nagle, J.F., 1989. Structure of the fully hydrated gel phase of dipalmitoylphosphatidylcholine. Biophys. J. 55, 315–325.
Williams, J.H., Kuchmak, M., Witter, R.F., 1966. Fatty acids in phospholipids isolated from human red cells. Lipids 1, 391–398.
Vink, S.R., van Blitterswijk, W.J., Schellens, J.H.M., Verheij, M., 2007. Rationale and clinical application of alkylphospholipid analogues in combination with radiotherapy. Cancer Treat. Rev. 33, 191–202.
Yamamoto, N., Ngwenya, B.Z., 1987. Activation of mouse peritoneal macrophages by lysophospholipids and ether derivatives of neutral lipids and phospholipids. Cancer Res. 47, 2008–2013.
Zachariasen, W.H., 1945. Theory of X-ray Diffraction in Crystals. Dover Publications, Mineola, NY.